

## **EXPERIMENTAL OBSERVATION OF COLLISIONS OF NONLINEAR ENVELOPE PULSES IN LEFT-HANDED TRANSMISSION LINES PERIODICALLY LOADED WITH SCHOTTKY VARACTORS**

**K. Narahara<sup>\*</sup> and Y. Yamane**

Graduate School of Science and Engineering, Yamagata University, 4-3-16 Jonan, Yonezawa, Yamagata 992-8510, Japan

**Abstract**—We investigate experimentally the collisions of nonlinear envelope pulses in a left-handed transmission line with regularly spaced Schottky varactors. By measuring the test line, we successfully observed that when two nonlinear envelope pulses traveling in opposite directions collide, two new envelope pulses are developed. These new pulses satisfy the phase-matching condition, and their carrier wave frequencies are the sum of the carrier wave frequencies of the original pulses. This article describes the experimental observations, together with the fundamental properties and numerical performance prospects of the test line.

### **1. INTRODUCTION**

Recently, it was found that the collision of two nonlinear envelope pulses in composite right- and left-handed (CRLH) transmission lines periodically loaded with Schottky varactors leads to the development of a pair of envelope pulses (one traveling in the forward direction and the other in the backward direction) [1]. CRLH lines [2] are able to manage the dispersive properties of propagating waves [3, 4]. They have also received attention as the platform for the development of nonlinear envelope pulses [5–10]. The dispersion of CRLH lines can be compensated by the nonlinearity introduced by the varactors, resulting in a soliton-like envelope pulse. The collision-generated pulses can widen the application of nonlinear pulses in microwave and millimeter-wave engineering.

It is well known [11] that the efficiency of harmonic-wave generation in two-wave mixing is maximized, when the phase-matching

---

*Received 18 October 2011, Accepted 4 December 2011, Scheduled 11 December 2011*

\* Corresponding author: Koichi Narahara (narahara@yz.yamagata-u.ac.jp).

condition is satisfied. This condition is given by

$$k_3 \sim m_1 k_1 + m_2 k_2, \quad (1)$$

where  $k_1$  and  $k_2$  represent the wave numbers of incident waves, and  $k_3$  represents the wave number of the newly generated harmonic wave. Moreover,  $m_1$  and  $m_2$  are integers that are specified by the order of the generated harmonics. When the incident pulses have a common carrier frequency and are traveling in opposite directions, it results in the condition  $k_1 = -k_2$ . Hence, the maximal second harmonic generation can be observed when  $k_3 \sim 0$ . Consider the dispersion relationship of CRLH lines. For left-handed waves, there exists an upper-most cut-off frequency, called  $\omega_l$ , which corresponds to a wave number of zero. Hence, nonlinear pulses having a carrier frequency of  $\sim \omega_l/2$  can generate second harmonic pulses effectively using collisions. On the other hand, in the case when the carrier frequencies of two colliding pulses become unequal, the second harmonic envelope pulse travels mainly to the left (right) if  $k_3 > (<)0$ . In addition, the carrier frequency of the collision-generated pulses is the sum of the frequencies of the original pulses.

The purpose of this paper is to experimentally validate these calculations in relation to the collision-generated pulses. It is desirable that we can fix erroneous operations by reformation of the test circuit and detect easily voltages at any cells. We thus employed a standard breadboard. As a penalty of the advantages, the experiments had to be carried out at MHz frequencies, being much smaller than the frequencies at which the left-handed lines are utilized in free-space applications such as the new-type leaky-wave antenna discussed previously [1]. Moreover, we eliminated the series inductors from the test line to minimize the wave attenuation caused by the parasitic resistors. As a result, the test line did not exhibit right-handedness at any frequency bands. On the other hand, we could observe clearly the fundamental properties of the collision-generated pulses including the efficiency of the phase-matching condition.

First, we describe the fundamental properties of the test line used for the experiments, including the line structure, equivalent representation, and dispersion relationship. We then describe several results obtained by the experiments. We observed the development of collision-generated pulses. Furthermore, the relationship between the wave numbers and carrier frequencies for the colliding and newly developed pulses was evaluated to examine whether the phase-matching condition determines the properties of the newly developed pulses.

## 2. FUNDAMENTAL PROPERTIES OF THE TEST LEFT-HANDED LINE

Figure 1(a) shows the representation of the unit cell for the test line we investigated experimentally. The series capacitor and shunt inductor are represented by  $C_L$  and  $L_L$ , respectively.  $R_i$  shows the parasitic resistance of the inductors. As mentioned above, the dispersion relationship of the test line does not have the right-handed branch, which appears in the CRLH lines' dispersion relationship. To introduce the nonlinearity, the shunt capacitor is replaced with a Schottky varactor  $C_R$ , whose capacitance-voltage relationship is generally given by

$$C(V) = \frac{C_0}{\left(1 - \frac{V}{V_J}\right)^M}, \quad (2)$$

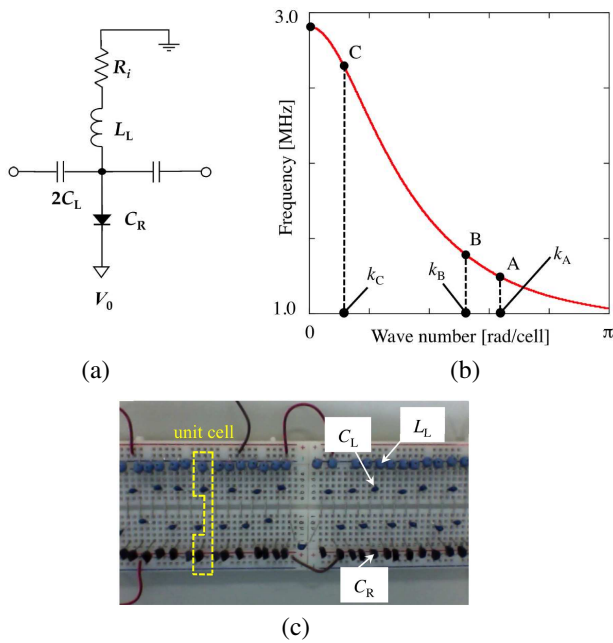


**Figure 1.** Properties of the test left-handed line. (a) The unit-cell structure, (b) the dispersion relationship, and (c) the photograph of the test line investigated experimentally. In Fig. 1(b) the wave number corresponding to the points  $A$ ,  $B$ , and  $C$  is represented by  $k_A$ ,  $k_B$ , and  $k_C$ , respectively.

where  $V$  represents the terminal voltage and  $C_0$ ,  $V_J$ , and  $M$  are the zero-bias junction capacitance, junction potential, and grading coefficient, respectively. We consider a situation where each Schottky varactor was biased at  $-V_0$  ( $V_0 > 0$ ). For convenience, we define  $C_R^{(0)}$  as  $C_R^{(0)} \equiv C(-V_0) = C_0/(1 + V_0/V_J)^M$ .

Using these variables, the long-wavelength dispersion relationship  $\omega = \omega(k)$  is expressed as [12]

$$\omega(k) = \frac{1}{\sqrt{C_L L_L \left( \frac{C_R^{(0)}}{C_L} + k^2 - \frac{k^4}{12} + \frac{k^6}{360} \right)}}, \quad (3)$$

where  $\omega$  and  $k$  represent the angular frequency and wave number, respectively. Fig. 1(b) shows the sample dispersion relationship obtained using the line parameters listed in Table 1 and setting  $V_0$  to 3.0 V. The line has a cut-off frequency  $f_u$ , which corresponds to the zero wave number, and exhibits a left-handed property. Presently,  $f_u$  is calculated to be 2.9 MHz.

### 3. EXPERIMENTS

Figure 1(c) shows the photo of a one-dimensional left-handed line used for the measurements. The circuit was built on a standard breadboard. The Schottky varactors used were TOSHIBA 1SV101 diodes. Shunt inductances and series capacitances were implemented using 100  $\mu\text{H}$  inductors (TDK EL0405) and 47 pF capacitors (TDK FK24C0G1), respectively. The values in Table 1 simulate the test line, which was fed by pulse signals generated by an NF WF1974 two-channel arbitrary waveform generator. An envelope pulse with a triangle waveform were input at both ends of the line, and the pulse widths were set to include 20 cycles of the carrier sinusoidal wave. The pulse's bandwidth was in most cases 0.2 MHz for the frequencies we used. The signals along the test line were detected using Agilent 10073C passive probes and were monitored in the time domain using an Agilent DSO90254A oscilloscope. The test line was already validated to ensure that it

**Table 1.** Line parameters used for numerical evaluations of the test line.

|       |                   |       |       |
|-------|-------------------|-------|-------|
| $C_L$ | 47 pF             | $M$   | 1.26  |
| $L_L$ | 100 $\mu\text{H}$ | $V_J$ | 3.6 V |
| $R_i$ | 20.0 $\Omega$     | $C_0$ | 65 pF |

has the expected dispersive properties [12]. As expected, the parasitic resistance of the inductors was significant; therefore, the attenuation constant was estimated to be  $1.5 \times 10^{-2}$  nepers/cell. This attenuation results in limited contribution of nonlinearity.

We first tried to detect the collision-generated pulses. We set  $V_0$  to 3.0 V. Envelope pulses having carrier frequencies of 1.25 MHz and 1.40 MHz were applied at the left and right ends, respectively. Hence, the right- and left-going pulses occupy the points  $A$  and  $B$ , respectively, in Fig. 1(b). The sum-frequency ( $= 2.65$  MHz) corresponds to point  $C$ . The wave numbers  $k_A$ ,  $k_B$ , and  $k_C$  were calculated to be 1.98, 1.62, and 0.36 rad/cell, respectively. This means that the phase-matching condition was well satisfied, i.e.,  $k_A - k_B \sim k_C$ . Moreover, the collision-generated pulse was supposed to travel to the right. The total cell number was set to 105. Although this cell number was sufficiently small to avoid excessive wave attenuation which disables the nonlinearity, the small cell number made it difficult to secure the time window to differentiate between the incident and collision-generated pulses. However, there was sufficient separation between these two pulses in the frequency domain because the collision-generated pulses have a sum-frequency carrier. We therefore performed the Fourier-transform operation on the measured temporal waveforms and operate band-pass filters to separate the incident and collision-generated pulses in the frequency domain. Then, the separated time-domain waveforms were obtained by inverse Fourier transform.

Figure 2 shows the measurement results. Six different spatial waveforms are plotted with temporal increments of  $2.0 \mu\text{s}$ . The red and blue waveforms represent the incident and collision-generated pulses, respectively. In Fig. 2(a), the right- and left-going incident pulses start to collide. It was found that longer-wavelength pulses are consistently generated by collisions and start to travel to the right, as we can see in Figs. 2(b)–(f), where arrows are attached to the collision-generated pulses. We performed the Fourier-transform operation on the measured spatial waveform and obtained Fig. 3. Three peaks in the spectrum corresponded to the carrier waves of the incident and collision generated pulses. The wave numbers of the left- and right-going incident pulses were estimated to be 1.56 rad/cell and 1.86 rad/cell, respectively. Moreover, the collision-generated pulse had the wave number of 0.30 rad/cell, which was coincident with the difference between the wave numbers of the left- and right-going incident pulses.

We then varied the carrier frequency of the pulse applied to the left end called  $f_r$ , from 1.0 MHz to 1.8 MHz with 0.05 MHz increments, while the carrier frequency was kept fixed at 1.4 MHz for the pulse

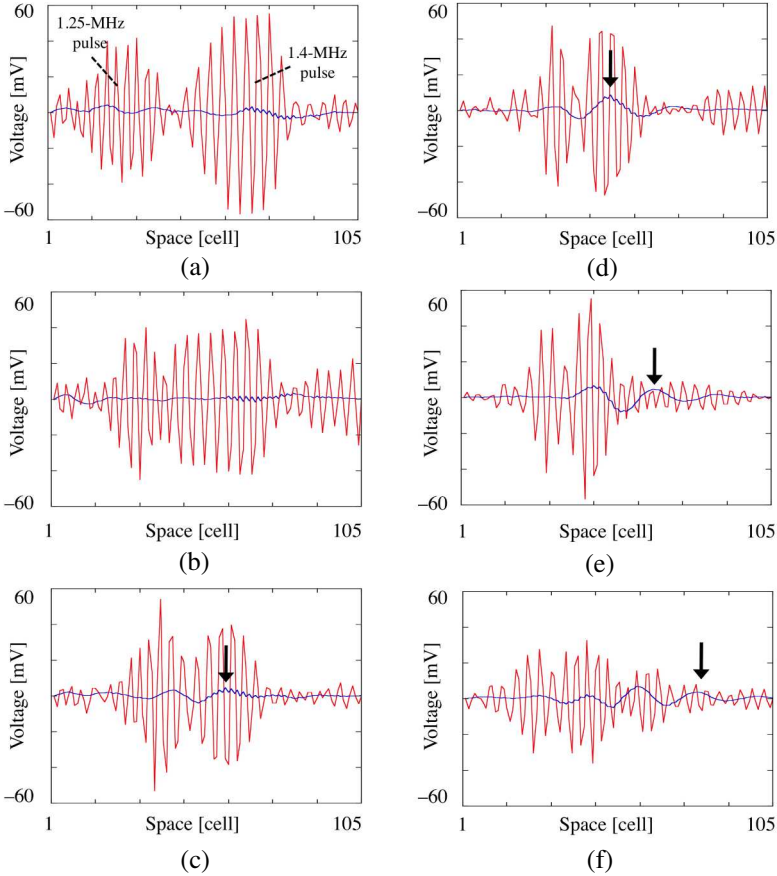


**Figure 2.** Measured spatial waveforms. The red and blue waveforms represent the incident and collision-generated pulses, respectively. The figures are in order of increasing time with 2.0- $\mu$ s increments.

applied to the right end. To characterize the collision-generated pulses, we use two quantities: the spectral power and the central frequency. These two are respectively defined by  $P = \int_{f_b}^{f_t} |S(f)|df$  and  $f_c = \int_{f_b}^{f_t} f|S(f)|df/P$ , where  $S(f)$  represents the Fourier amplitude of the frequency  $f$ . In addition,  $f_b$  and  $f_t$  are respectively the lower and higher cutoff frequencies of the band-pass filter used to extract the Fourier components corresponding to the collision-generated pulses. The black curves in Figs. 4(a) and (b) represent  $P$  and  $f_c$ , which were obtained by recording and Fourier-transforming the waveforms at  $n = 50$ . The dashed line in Fig. 4(b) represents the positions

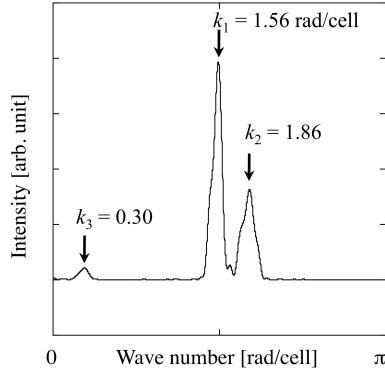


**Figure 3.** Measured wave numbers.  $k_1$  and  $k_2$  represent the wave numbers of the left- and right-going incident pulses, and  $k_3$  represents that of the collision-generated pulse.

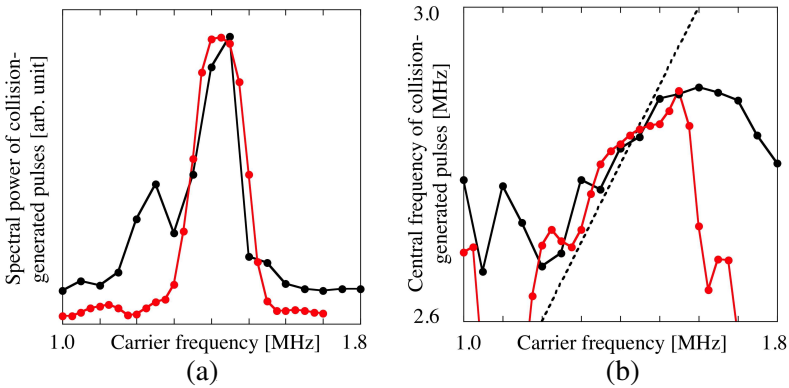


**Figure 4.** Collision of nonlinear envelope pulses, whose carrier frequencies differ from each other. The carrier frequency of the leftgoing pulse is fixed at 1.4 MHz, while that of the right-going pulse is varied from 1.0 MHz to 1.8 MHz with 0.05-MHz increments. (a) The spectral power and (b) the central frequency of the collision-generated pulses. Black and red curves represent the measured and calculated dependences, respectively.

of the sum-frequency. We can see that  $P$  becomes significant from  $f_r = 1.2$  MHz to 1.55 MHz and maximal at  $f_r = 1.45$  MHz. For these frequencies,  $f_c$  becomes close to the sum-frequency line. For  $f_r \geq 1.5$  MHz, the sum-frequency may surpass  $f_u$ , such that the collision-generated pulses have to be strongly suppressed. This results

in an abrupt decrease in  $P$  between  $f_c = 1.45$  and  $1.5$  MHz. On the other hand, for  $f_r < 1.2$  MHz, the corresponding wave number becomes much larger than that at  $f_r = 1.4$  MHz. Therefore, the phase-matching condition cannot be satisfied, irrespective of what frequencies are included in the pulse bandwidth.

The black curves in Fig. 5 represent another measured frequency dependence of  $P$  and  $f_c$ . Presently, the carrier frequencies of the incident pulses  $f_{rl}$  are varied from  $1.26$  to  $1.54$  MHz with  $0.01$  MHz increments such that both the right- and left-going pulses have an identical frequency. As in Fig. 4, Figs. 5(a) and (b) show  $P$  and  $f_c$  that are obtained by recording and Fourier-transforming waveforms at  $n = 50$ . The dashed line in Fig. 5(b) corresponds to the second harmonic frequency. We can see that  $P$  becomes maximal at  $f_{rl} = 1.43$  MHz, where  $f_c$  coincides exactly with the second harmonic frequency. Moreover, for  $f_{rl} < (>)1.43$  MHz,  $f_c$  becomes greater (less) than the second harmonic frequency. The small discrepancy between  $f_c$  and the second harmonic frequency suggests that the proper frequency components of the incident pulses contribute to the generation of second harmonic pulses. The black curves in Figs. 6(a) and (b) show the measured dependence of  $P$  and  $f_c$  on  $V_0$ . Both the right- and left-going incident pulses have a  $1.4$ -MHz carrier frequency. We can see that  $P$  becomes maximal at  $V_0 = 3.0$  V, which suggests that at this bias voltage, phase matching is mostly satisfied. For other bias voltages,  $f_u$  becomes varied. This alteration in dispersion results in the violation of the phase matching condition and explains the decrease in

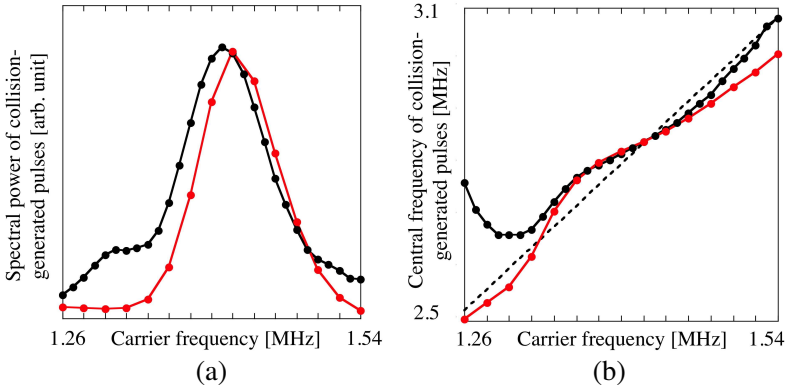


**Figure 5.** Collision of nonlinear envelope pulses having identical carrier frequency. (a) The spectral power and (b) the central frequency of the collision-generated pulses. Black and red curves represent the measured and calculated dependences, respectively.

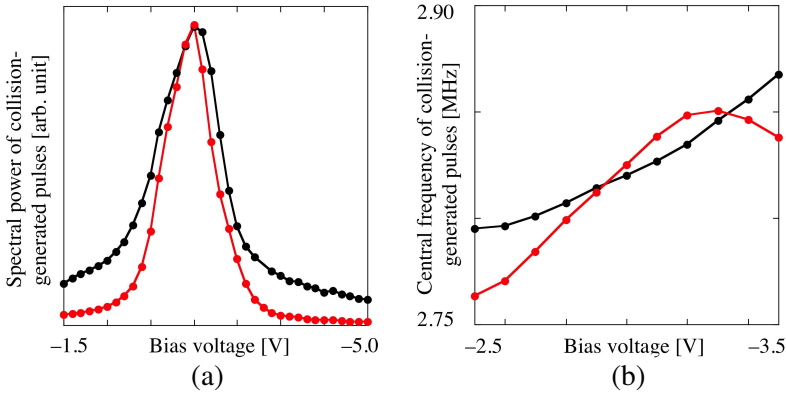


**Figure 6.** Properties of collision-generated pulses for different bias voltages. The carrier frequencies of left- and right-going pulses are both set to 1.4 MHz. (a) The spectral power and (b) the central frequency of the collision-generated pulses. Black and red curves represent the measured and calculated dependences, respectively.

$P$  for these bias voltages. In Fig. 6(b),  $f_c$  increases as  $V_0$  increases. The carrier frequency of the collision-generated pulses can be managed by changing  $V_0$ .

#### 4. DISCUSSION

To predict the behavior of collision-generated pulses, we numerically solve the transmission equations given by

$$C_L \frac{d}{dt} (V_{n-1} - V_n) = I_n, \tag{4}$$

$$L_L \frac{d}{dt} \left[ C(V_n - V_0) \frac{dV_n}{dt} \right] = -R_i C(V_n - V_0) \frac{dV_n}{dt} - V_n + \left( L_L \frac{d}{dt} + R_i \right) (I_n - I_{n+1}), \tag{5}$$

where  $V_n$  and  $I_n$  show the line voltage and current, respectively, at the  $n$ th cell. The setup of the input signals and biasing voltage is the same as that of the measurements used to obtain Fig. 2.

That is, we use the values listed in Table 1 and set  $V_0$  to 3.0 V. Moreover, 1.25-MHz and 1.40-MHz envelope pulses are applied at the left and right ends, respectively. Fig. 7 shows six spatial waveforms with 2.0- $\mu$ s increments. We separate the incident and collision-generated pulses using the above-mentioned flow. The red and

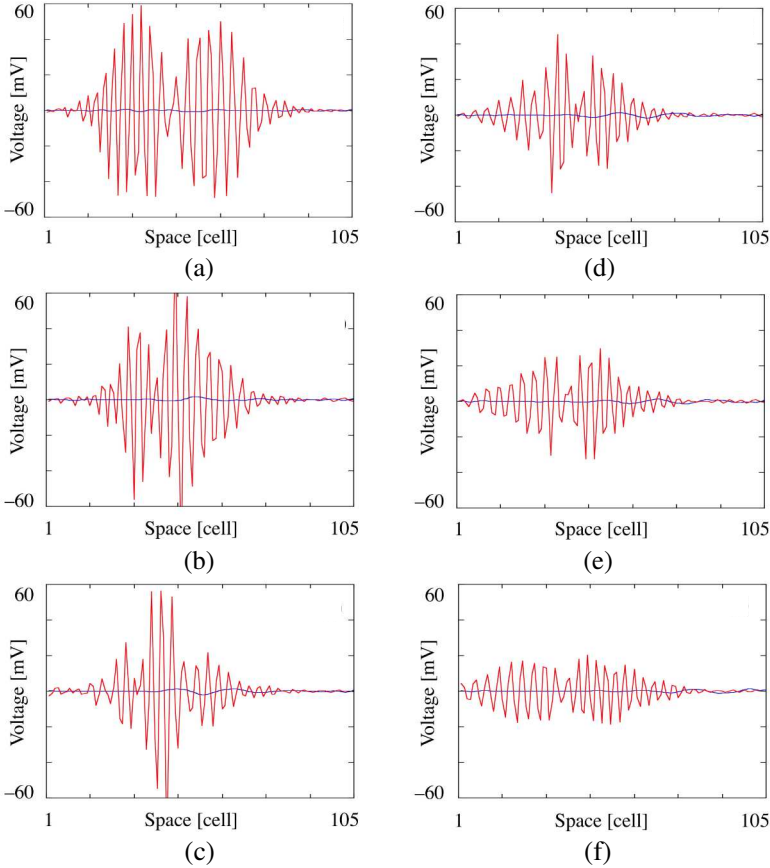


**Figure 7.** Calculated spatial waveforms. The red and blue waveforms represent the incident and collision-generated pulses, respectively. The figures are in order of increasing time with 2.0- $\mu$ s increments.

blue waveforms represent the incident and collision-generated pulses, respectively. We can clearly observe the development of a collision-generated longer-wavelength envelope pulse, which starts to travel to the right. The properties of the calculated collision-generated pulses are shown in Figs. 4 to 6 by the red curves. The similarity between the measured and calculated properties of the collision-generated pulses in Figs. 2 to 7 is sufficient to consider the numerical model as reliable model for the prediction of the behavior of nonlinear pulses. Using this numerical model, we evaluated the phase-matching condition. We set the total cell number and  $R_i$  to 1000 and 0.0  $\Omega$ , respectively. We performed the Fourier-transform operation on the calculated spatial

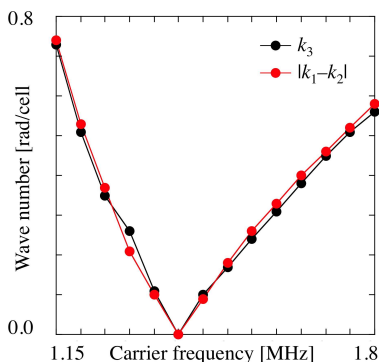


**Figure 8.** Phase-matching condition for the test lines.  $k_{1,2}$  and  $k_3$  represent the wave numbers of the incident and collision-generated waves, respectively.

waveforms. Fig. 8 shows the result. Red and black curves represent the separation of the wave numbers corresponding to the incident carrier waves and the wave number of the collision-generated carrier waves, respectively. It was clearly seen that  $k_3 \sim |k_1 - k_2|$ , so that the phase-matching condition governed the properties of the collision-generated pulses.

## 5. CONCLUSION

We experimentally characterized the collision of nonlinear envelope pulses in left-handed transmission line that are periodically loaded with Schottky varactors. We explicitly observe collision-generated pulses whose carrier frequencies are given by the sum of the incident pulses. It was also established that the phase-matching condition determines the efficiency of obtaining large collision-generated pulses. Moreover, numerical calculations using a simplified model of the line well simulated the measured results.

## REFERENCES

1. Narahara, K., "Collision of nonlinear envelope pulses developed in composite right- and left-handed transmission lines periodically loaded with Schottky varactors," *Progress In Electromagnetics Research C*, Vol. 21, 1–12, 2011.
2. Caloz, C. and T. Itoh, *Electromagnetic Metamaterials: Transmission Line Theory and Microwave Applications*, Wiley, 2006.

3. Monti, G. and L. Tarricone, "Signal reshaping in a transmission line with negative group velocity behaviour," *Microwave Optical Technol. Lett.*, Vol. 51, 2627–2633, 2009.
4. Chi, P. and T. Itoh, "Dispersion engineering with CRLH metamaterials," *Proc. IEEE International Symposium on Radio-Frequency Integration Technology*, 128–131, 2009.
5. Kozyrev, A. B. and D. W. van der Weide, "Nonlinear wave propagation phenomena in left-handed transmission-line media," *IEEE Trans. Microwave Theory and Techniques*, Vol. 53, 238–245, 2005.
6. Gupta, S. and C. Caloz, "Dark and bright solitons in left-handed nonlinear transmission line metamaterials," *Proc. IEEE MTT-S Int'l. Microwave Symp.*, 979–982, Honolulu, 2007.
7. Kafaratzis, A. and Z. Hu, "Envelope solitons in nonlinear left handed transmission lines," *Proc. Metamaterials 2007*, 22–24, 771–773, 2007.
8. Simion, S., R. Marcelli, G. Bartolucci, G. Sajin, and F. Craciunoiu, "Nonlinear composite right/left-handed transmission line for frequency doubler and short pulse generation," *Proc. Metamaterials 2008*, 492–494, 2008.
9. Gharakhili, F. G., M. Shahabadi, and M. Hakkak, "Bright and Dark soliton generation in a left-handed nonlinear transmission line with series nonlinear capacitors," *Progress In Electromagnetics Research*, Vol. 96, 237–249, 2009.
10. Ogasawara, J. and K. Narahara, "Short envelope pulse propagation in composite right- and left-handed transmission lines with regularly spaced Schottky varactors," *IEICE Electron. Express*, Vol. 6, 1576–1581, 2009.
11. Boyd, R. W., *Nonlinear Optics*, Academic Press, 2002.
12. Ogasawara, J. and K. Narahara, "Experimental characterization of left-handed transmission lines with regularly spaced Schottky varactors," *IEICE Electronics Express*, Vol. 7, No. 4, 608–614, 2010.